



Optimization of deep drawing products by adding effect of texture pattern in draw bead design

Mohammad Soroush Merhani¹ · Ali Parvizi²

Received: 25 February 2021 / Accepted: 15 December 2021 / Published online: 29 December 2021
© The Author(s), under exclusive licence to The Brazilian Society of Mechanical Sciences and Engineering 2021

Abstract

Draw beads, as an effective tool in sheet metal forming dies, play an important role in drawing the parts with complicated geometry. The quality of deep drawn parts could be improved by controlling the draw beads dimensions, including height, width and length in sheet metal forming dies. These parameters as well as the texture pattern of draw beads created by different machining strategies are considered as input parameters in this study to optimize the quality of drawn parts manufactured by deep drawing process. Three different texture patterns are introduced and the coefficient of friction related to each one is measured using a proposed method. The values of maximum residual stress, maximum plastic strain, maximum punch force, and wrinkling are chosen as output parameters defining the part quality. For case study, the deep drawing process of an industrial die is simulated using ABAQUS/Explicit software. Thereafter, the results of experimental investigation are used for verification of FE model. The effect of each parameter on the quality of drawn parts is investigated using response surface method (RSM). Then, the optimal values of input parameters are obtained by RSM technique. Additionally, the optimization of response surface is carried out using genetic algorithm (GA) contributing to improvement in the output parameters.

Keywords Deep drawing · Draw beads · Optimization · FEM · RSM

1 Introduction

Sheet metal forming, as one of the typical production processes for manufacturing automotive body parts, has many advantages such as low cost and high production rate. This makes it reasonable to be chosen in automotive industries, especially in press shops, in response to demands for high-quality parts. With gradual sophistication in the geometry of drawing parts, new components are exploited in drawing dies. For instance, new die parts called draw beads have been designed to control the sheet flow and its speed while applying a sufficient stretch force. During contact between sheet and bead, the restraining force of the draw bead is a combination of the force required for bending and reverse

bending of sheet (due to bead geometry), plus the force to overcome friction (due to contact of bead and sheet).

Draw beads and their effects on quality of drawn parts have been studied by various researchers. Li et al. [1] indicated that when the sheet is crossing the bead section, bending force, reverse bending force, friction force, and resistance created by strain hardening increase the extent of resistance to the blank feed. Hence, the blank feeds in different locations of die could be controlled by changing the bead dimension and location on die. Thipprakmas [2] examined the effect of bead width and height on quality of drawn parts. Concave/convex features of walls in deep drawing process are defined as quality of drawn parts. His results suggested that use of bead reduced the concave feature of wall. Phanitwong and Thipprakmas [3] investigated the effect of bead height and width on thinning of walls in deep drawing process. They showed that thinning in walls declines by increasing the width and reducing the height of bead. Therefore, it is important to determine the proper dimension of bead in order to obtain straight walls with minimum thinning in thickness.

Also, the extent of friction between bead and sheet has been investigated by a number of researchers. Schey [4] explored the effect of dissimilar bead coatings with

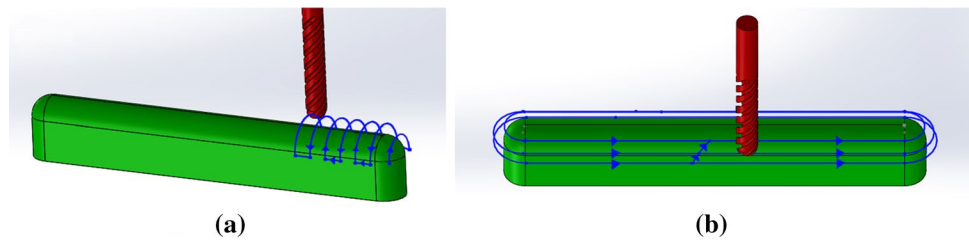
Technical Editor: Lincoln Cardoso Brandao.

✉ Mohammad Soroush Merhani
soroush.mergani@ut.ac.ir

¹ Department of Mechanical Engineering, College of Engineering, University of Tehran, Tehran, Iran

² School of Mechanical Engineering, College of Engineering, University of Tehran, Tehran, Iran

Fig. 1 Two strategies of tool pass for machining of bead **a** perpendicular to the bead axis **b** parallel to the bead axis



different lubricants. It was observed that although the friction in coated beads was relatively higher than in polished or grinded ones, the damages on sheets crossing the coated bead were reduced and the surface quality of parts improved.

Some researchers investigated another geometrical parameters of draw beads affecting deep drawing. Raghavan et al. [5] studied the effect of blank holder plane slope on draw bead restraining force. They found that the maximum draw bead restraining force was obtained in positive angles of blank holder plane relative to horizon. Smith et al. [6] obtained pulling and holding forces for draw bead on inclined surfaces. Using FEM and experimental test, Murali et al. [7] inspected the location of bead relative to the die edge. Reducing the stress and thinning in blank during deep drawing process were their criteria for locating the bead. Sheriff and Ismail [8] studied the proper location of bead with a rectangular cross section by finite element method using Dyna software. Reducing the thickness changes and maximizing the strain were the criteria considered for locating the bead.

A group of researchers used draw bead restraining force, as the main feature to design and optimize the draw bead. Chen and Liu [9] replaced draw bead restraining force as equivalent of draw bead in finite element simulation of stamping die. With the aim of improving the formability of blank in deep drawing process, Naceur et al. [10] optimized the restraining force of draw bead. A simplified finite element method was developed in which the draw bead restraining force was considered alongside the optimization algorithms for optimizing the restraining force. Wei and Yang [11] considered the blank holder force and draw bead restraining force as input parameters to optimize the design parameters such as failure, wrinkling, insufficient stretch, and thickness reduction in deep drawing process.

Some researchers inserted draw bead as input of optimization and used it to optimize the parameters that are important in drawing. Considering dimensional limitation of bead production, Sun et al. [12] presented a proper response surface for multi-objective optimization of bead in a Pareto front. Applying reverse computation method, Han et al. [13] determined maximum stress, stress and thickness deviations in a certain deep drawing die. Thereafter, a reverse neural network was taken into account to reach an optimal bead geometry, while the structure of neural network was

optimized by genetic algorithm. Han et al. [14] also introduced a modified Tikhonov procedure based on genetic algorithm for reverse computation of bead dimensions. Hu et al. [15] used Kriging method for bead design to reduce the failure probability of blank during deep drawing. Using FLD¹ and multi-objective genetic algorithm, Kardan et al. [16] optimized deep drawing process considering punch force and sheet thickness variation as output parameters of the study. They investigated the influence of eight main parameters of deep drawing by conducting experimental tests. Also, Kardan et al. [17] investigated the effect of deep drawing parameters on the residual stress of the final part. The study included experimental and FE simulation of a cylindrical die to minimize the residual stress in post-deep drawing process.

Having reviewed the literature in the field of deep drawing process, no research has addressed the texture pattern of draw beads as well as their dimensional parameters considered to improve the quality of the drawn part. Maximum residual stress, maximum plastic strain, maximum punch force, and maximum wrinkling are taken into account as criteria to define the quality of drawn part. Additionally, the process is wholly simulated in ABAQUS/Explicit software, while experimental results are carried out to evaluate the model. RSM method which is optimized by genetic algorithm (GA) is applied to attain the optimal values of input parameters. The developed knowledge could be utilized in sheet metal forming industries. It also gives vision about the effect of machining strategy (surface texture pattern) on function of a product.

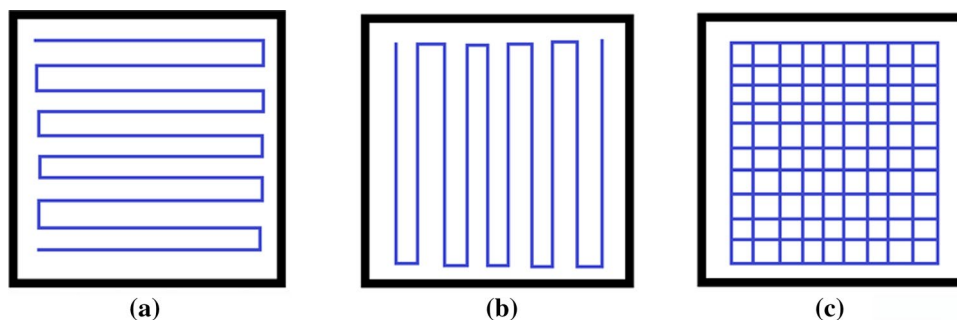
2 Experimental procedure

2.1 Measuring the coefficient of friction

In order to apply the effect of each texture pattern on finite element model, the coefficient of friction for each pattern was used. Texture patterns were created on bead surface during the machining process. Three different strategies of machining were taken into account for creating texture

¹ -Forming Limit Diagram.

Fig. 2 Tool path on test blocks for friction measurement **a** perpendicular to the bead axis **b** parallel to the bead axis **c** combined pattern



pattern on bead. Tool path in parallel and perpendicular machining relative to bead axis are demonstrated in Fig. 1. Indeed, the sheet moves perpendicular to the bead axis. In order to study the effect of machining strategy on texture pattern and resulting coefficient of friction, the same machining tool path was applied to a steel block, with the same material as bead. Three patterns comprising textures parallel with the bead axis, perpendicular to the bead axis, and their combination are illustrated in Fig. 2. Then, the coefficients of friction of sheets with block were measured.

Similar to the apparatus proposed by Lee et al. [18], a typical system for measuring the friction by clamping was designed to measure the coefficient of friction based on G115 ASTM standard [19]. As illustrated in Fig. 3, the idea of design comprises a uniaxial tensile test machine as well as a fixture for applying normal force to the contact surfaces. The materials for experiment were prepared in the form of block and sheet. Normally, sheet sample is fixed to the upper grip of tensile test machine and is held between two blocks with the same material of bead. By applying displacement to the upper grip, tensile test machine records measured force for each extent of sheet displacement. Designed fixture was fixed in the lower grip of tensile test machine. This fixture held the sheet by applying normal force to blocks in contact with the sheet. During the experiment, friction force was measured by load cell of tensile test machine, while normal force of blocks was measured by load cell placed in fixture.

Clamping force in each experiment was set to be 10 kg and displacement speed was 5 mm/min. Having values of friction (shear) and clamping (normal) forces, coefficient of friction in each case was calculated as follows:

$$\mu = \frac{\text{Friction force}}{2 \times \text{Clamping force}} \quad (1)$$

Figure 4 presents the plot of friction coefficients concerning each texture pattern. In each case, the mean values of coefficient of friction calculated in steady-state condition, i.e., 0.18, 0.195, and 0.22 were considered as empirical value for vertical, parallel, and square texture patterns, respectively.

Slippage at the beginning parallel sample in Fig. 4 of friction test refers to unfavorable contact or clamping conditions. Although slippage happened at the beginning the rest of diagram showed a steady situation which means, during dynamic sliding, the amount of dynamic friction coefficient is stable and reliable, so it is used in simulation.

2.2 Design of experiment

Design-Expert software was used to design a table of experiments to study draw bead texture pattern beside the geometric parameters of draw bead. The examined bead had semi-circular cross section called circular bead. Four parameters of texture pattern (μ), height, width, and length of bead were chosen as input variables of design with three levels

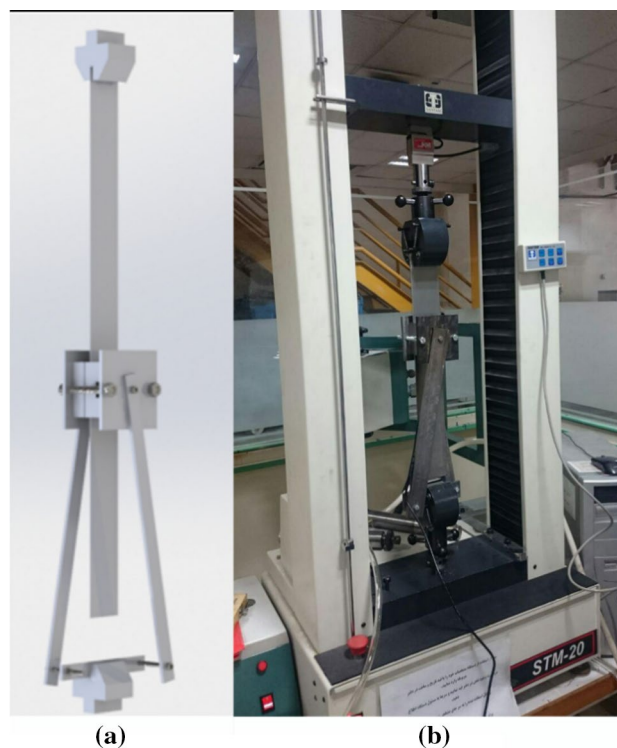
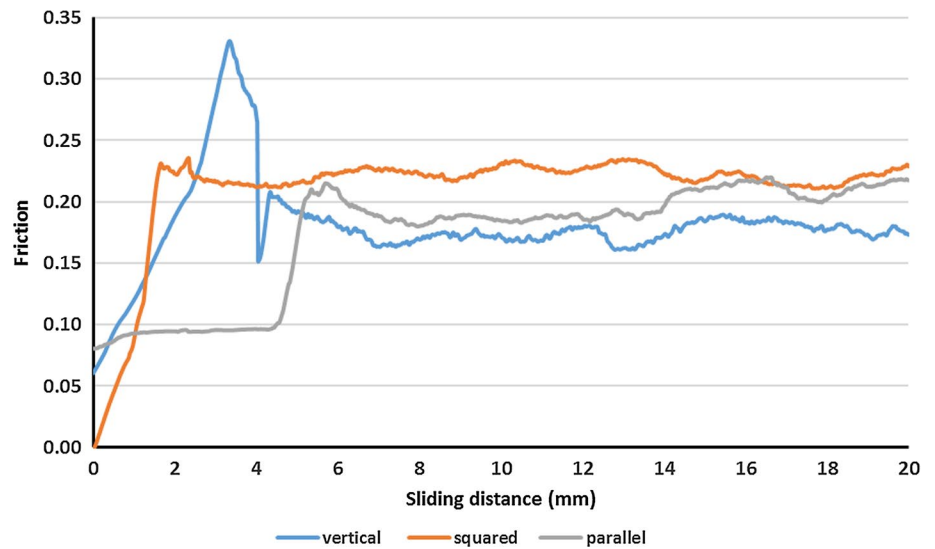


Fig. 3 **a** 3D model of fixture **b** tensile test machine set up for clamping the sheet with blocks

Fig. 4 Friction coefficients measured by test set up for different texture patterns



considered for each parameter. Three parameters of height, width, and length were continuous variables so the beginning and ending of their range were set as the first and last level and automatically the middle of the range was taken as the middle level of input parameter, but the texture pattern was a discontinuous variable. In order to enter the levels of μ in three texture patterns as a discontinuous parameter, type of μ in input parameters was considered as category. Table 1 shows each input parameter with its range or levels. Design-Expert suggested RSM method with a table of experiments including 51 experiments for the parameters defined in Table 1.

Experiment 14 from the designed table of experiments had the same draw bead dimensions in comparison with draw beads installed on a deep drawing die used for manufacturing a truck part called "Long Arm." So, the mentioned die was used for the experimental test. The result of this test was compared with the results of FEM obtained from simulation of drawing process in ABAQUS. The dimension of part after spring back and residual stress after drawing process were measured on the part and model. After comparing the results of measurements and evaluating the model, the whole 51 experiments suggested by Design-Expert were simulated using ABAQUS software. Figure 5 depicts long arm drawing die consisting of (a) punch with blank holder and (b) die with draw beads on die surface. According to this figure, the die includes 2 pairs of beads on longitudinal direction and one single bead on top of the part.

The initial blank with a size of 210*950 mm and thickness of 1 mm was prepared for the drawing process. Figure 6 displays the drawn part produced by the drawing process.

The maximum residual stress, maximum thinning, maximum punch force, and wrinkling on the edge of blank after unloading and spring back were selected as the process outputs for improving the quality. Further, the maximum

distance between blank edge and holder surface after unloading was considered as the criterion for wrinkling. The criteria for measurement of wrinkling were selected as the maximum amplitude of wave created on the blank edge. Also, the area of measurement was the space between beads on each side of the die. Zero wrinkling situation in this definition was the time when no wave was created on the edge of blank and the part lied completely on the flat surface of holder where no section of it loses its contact with the holder.

3 Finite element modeling

3.1 Material properties

The material used for deep drawing was considered as ductile material with strain hardening, anisotropy in plastic region, and ductile failure. In order to extract the material properties of sheet including modulus of elasticity, stress-strain curve, and anisotropy coefficient, uniaxial tensile test was conducted on sheet samples. The dimensions of samples were chosen from ASTM E8 standard and they were prepared in three directions of parallel, perpendicular, and angle of 45° with the direction of rolling. These samples

Table 1 Input parameters with selected levels for each parameters

Parameter	Level 1 (code - 1)	Level 2	Level 3 (code + 1)
Texture pattern (μ)	0.18	0.195	0.22
Height of bead (mm)	3	-	7
Width of bead (mm)	7	-	13
Length of bead (mm)	150	-	200

Fig. 5 Set of **a** punch and blank holder **b** die and beads

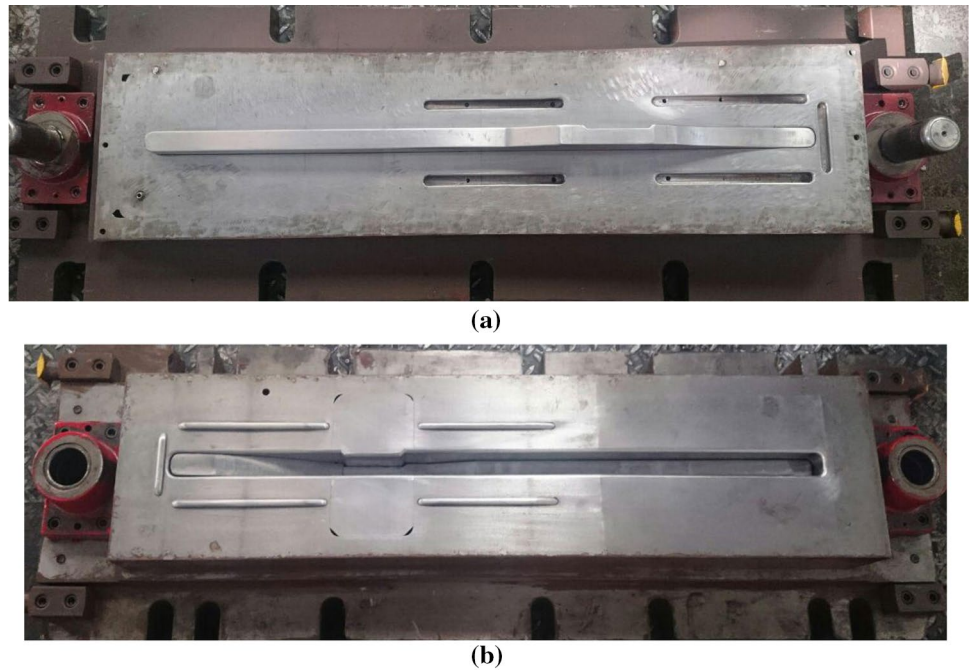
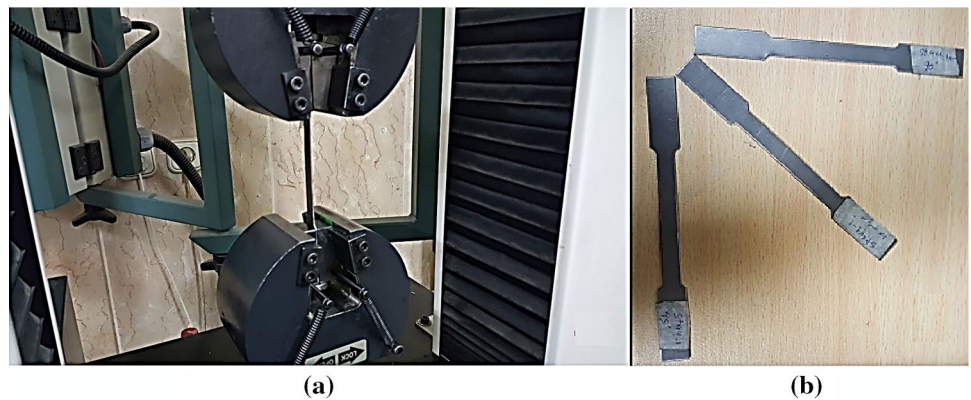


Fig. 6 Drawn part according to experiment 14



Fig. 7 **a** Tensile test based on ASTM E8 **b** samples in three directions of parallel, perpendicular and angle of 45° relative to rolling direction



and stress–strain tests are shown in Fig. 7. The samples had thickness of 1 mm and tested with a strain rate of 0.001 s^{-1} .

Figure 8 reveals the plot of stress versus strain for three samples with the results of tensile test for three samples reported in Table 2. In order to calculate the energy required for ductile failure, the area under the curve in stress–strain

diagram was used. Area of calculation started from UTS^2 point and ended at the last point of data collection. The calculation was conducted by MATLAB software. The data of stress–strain collected from plastic deformation region, naturally included plastic hardening. So, the stress–strain table of plastic region was used straightly in FEM.

² - Ultimate Tensile Stress.

Fig. 8 Stress–strain curves for three samples

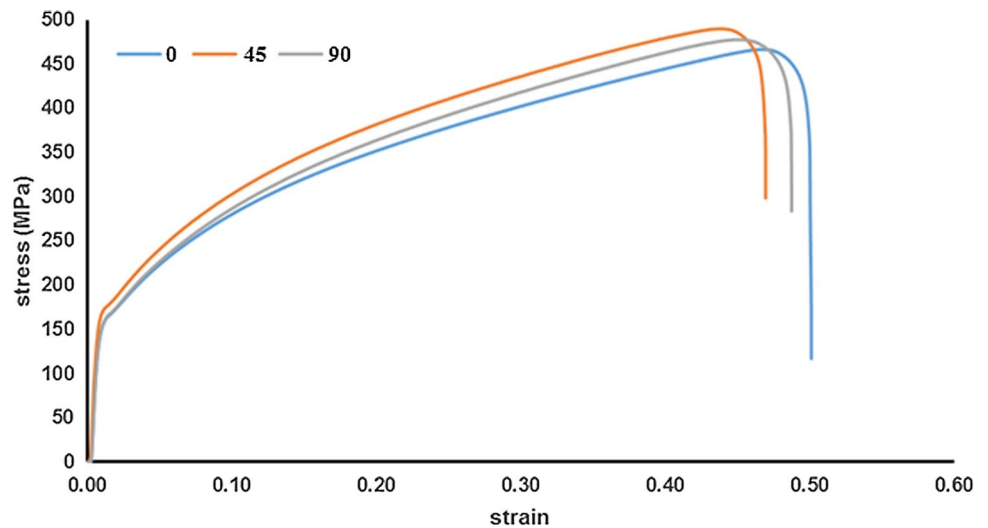


Table 2 Mechanical properties of deep drawn material obtained by uniaxial tensile test

	0°	45°	90°
Yields stress (MPa)	158	166	154
Ultimate stress (MPa)	465	490	470
Modulus of elasticity (GPa)		210	
Density (kg/m ³)		7800	
Poisson ratio		0.33	

Table 3 Friction coefficients applied on die surfaces

Rigid surface (master)	Deformable surface (slave)	μ		
Punch	Back side of blank	0.2		
Die	Front side of blank	0.2		
Holder	Back side of blank	0.2		
Beads	Front side of blank	0.18	0.195	0.22

Coefficient of anisotropy is calculated using Eq. (2):

$$R = \frac{\epsilon_y}{\epsilon_t} \tag{2}$$

In Eq. (2) ϵ_y refers to strain in transverse direction of calculation and ϵ_t refers to strain in thickness deformation. Parameter R can be calculated in 3 directions (0°, 45° and 90° relative to rolling direction). ABAQUS software calculates anisotropy with 6 coefficients that can be obtained by Eqs. (3)–(6):

$$R_{22} = \sqrt{\frac{R_{90}(R_0 + 1)}{R_0(R_{90} + 1)}} \tag{3}$$

$$R_{33} = \sqrt{\frac{R_{90}(R_0 + 1)}{(R_{90} + R_0)}} \tag{4}$$

$$R_{12} = \sqrt{\frac{R_{90}(R_0 + 1) \times 3}{(2 \times R_{45} + 1)(R_0 + R_{90})}} \tag{5}$$

$$R_{11} = R_{13} = R_{23} = 1 \tag{6}$$

In Eqs. (3) and (5) R_0 , R_{45} and R_{90} refer to calculation of Eq. (2) in direction of 0°, 45° and 90° relative to rolling direction sheet metal.

3.2 Contact surfaces and friction

First, contact surfaces of the die (punch, die, holder, and beads) and blank (front and back sides) were chosen and named individually. Then, according to DOE, coefficient of friction of beads in each experiment was selected from tables of friction coefficients. Table 3 summarizes the values of friction with contacting surfaces.

3.3 Assembly and mesh

In this section, die components were imported in assembly environment and placed in proper positions relative to each other. Figure 9 presents the separated parts of die in the assembly environment of ABAQUS.

In order to avoid unnecessary increase in the number of elements for flat surfaces of punch, holder, and die, the mesh

Fig. 9 Components of die in assembly module of ABAQUS

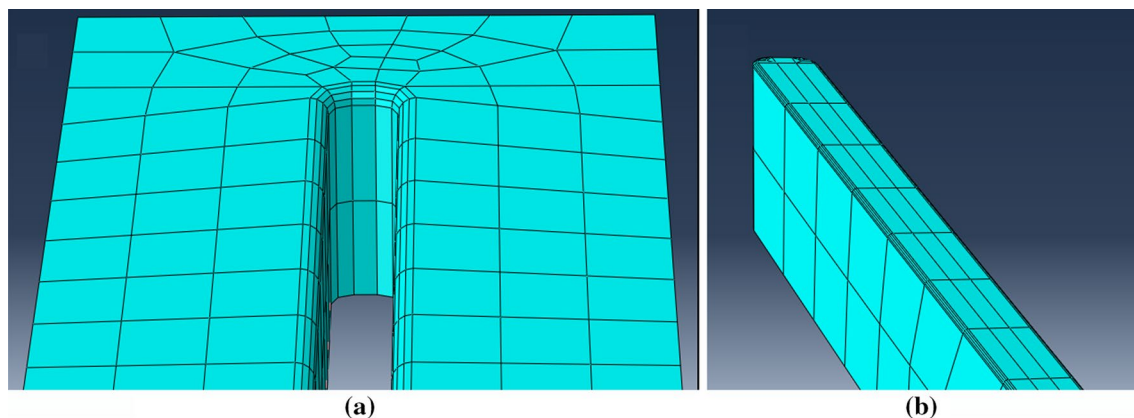
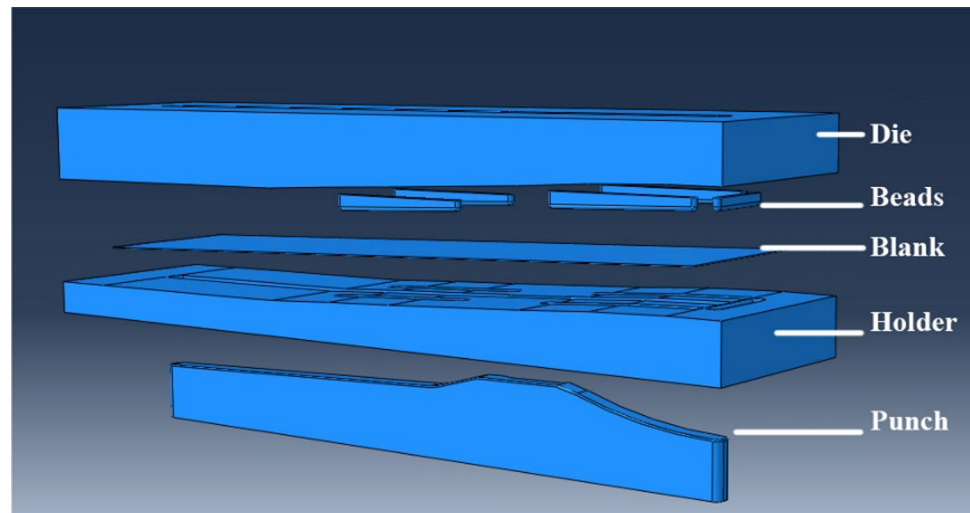


Fig. 10 Parts of meshed surfaces of **a** die **b** punch

Table 4 Element type and number of mesh in each instance

Instance	Element Type	Number of mesh	Weight (kg)
Die	R3D4	1586	170
Punch	R3D4	1060	20
Holder	R3D4	1550	140
Bead	R3D4	1864	0.2
Blank	C3D8R	49,874	Density (7800 kg/m ³)

size was set as 40*40 mm. However, for fillet radii of die and punch, the number of elements created on the edge was set as 4. The element type of R3D4 was selected for rigid parts and C3D8R for blank. The meshing process was carried out automatically by software. Figure 10 demonstrates a section of meshed surfaces of the die and punch. After applying different mass scales and comparing the internal energy and kinetic energy diagrams, mass scale of 500 was selected for the model. Table 4 summarizes the information on the mesh of instances.

In order to discover an appropriate mesh size for the blank, different mesh sizes were applied to it. Initially, finite element model was run with a rough mesh size (5×5 mm) for the blank. Then, according to the results of the current simulation, the mesh size in the next simulation was reduced. Due to lack of material flow on the bead in 5×5 mm mesh size, the simulation predicted failure on the blank. Hence, the mesh size was reduced to 2×2 mm step by step. The mesh size of 2×2 mm was adopted for the blank, since reduction in mesh size beyond this size caused dramatic increase in the computation time. Figure 11 shows the effect of mesh size on the finite element model.

4 Evaluation of finite element model

For evaluating the finite element model, spring back of drawn part (wall distances and blank edge distances) were measured and compared with the model. First, the distances between two vertical walls of the drawn part were

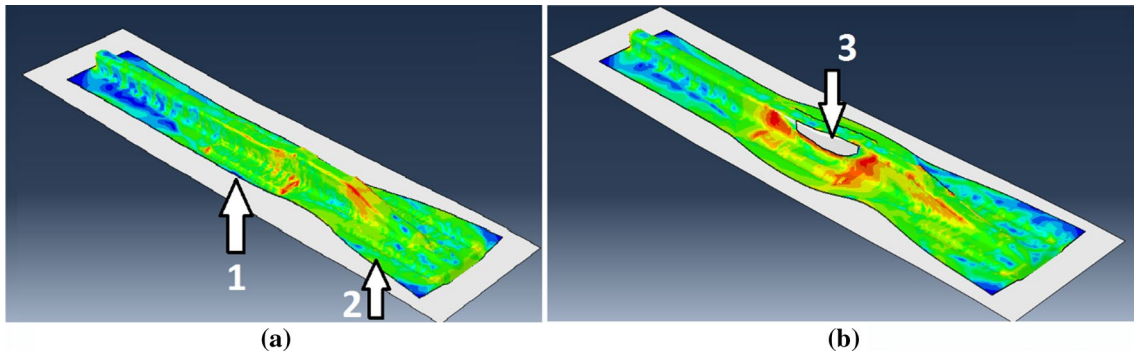
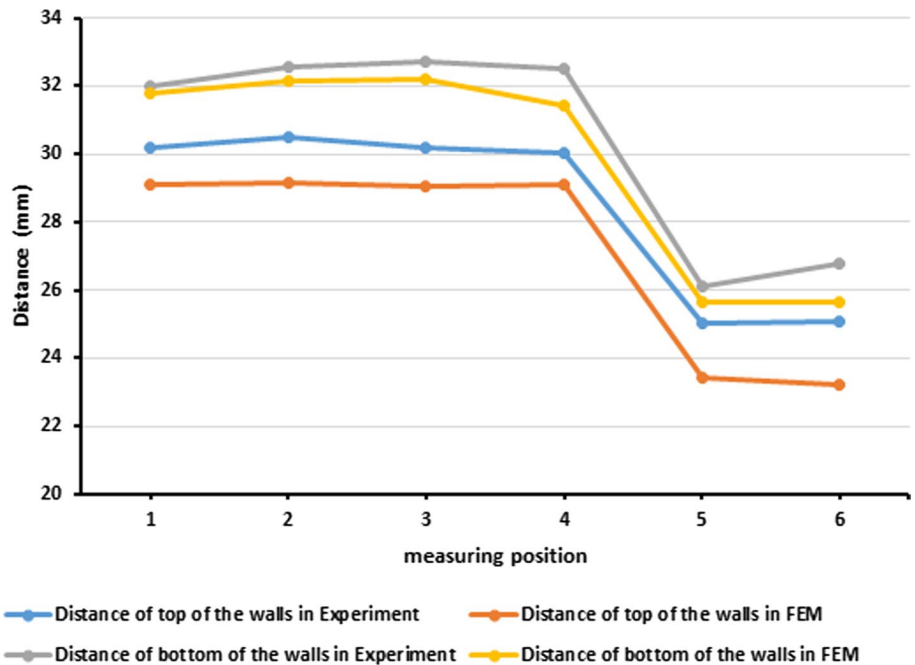


Fig. 11 Modeling deep drawing process with different mesh sizes **a** mesh size 2×2 mm **b** mesh size 5×5 mm, arrows 1 and 2: bead locations on die, arrow 3: failure location in mesh size 5×5 mm



Fig. 12 Positions of measuring points on drawn walls at 6 locations **a** experiment **b** finite element model

Fig. 13 Comparison of distance measurements in FEM and experiment

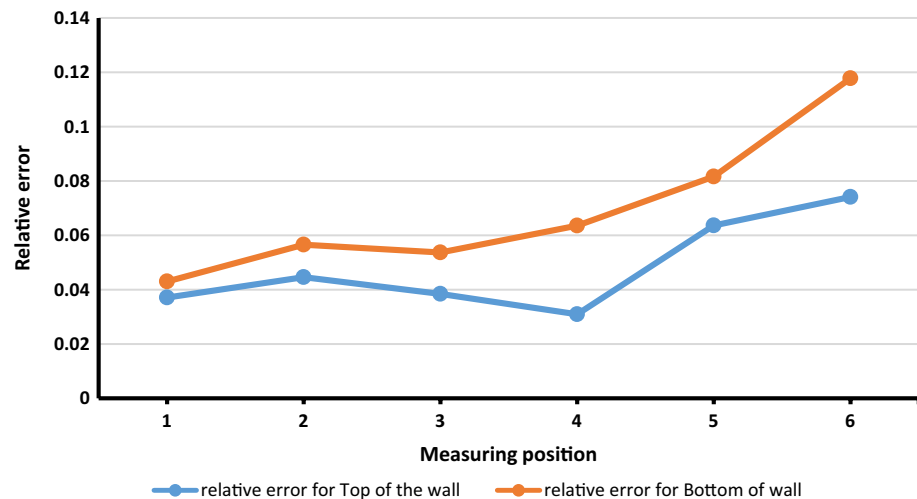


measured in 6 points. The positions of measured points were at the top and down of walls as shown in Fig. 12. Distances were measured using a caliper with an accuracy

of 0.05 mm, with the results reported in Fig. 13. Collected data from measurement are represented in Table 5.

Table 5 Walls distances in drawn part in experiment and FEM

Measuring position	Top of the walls			Bottom of the walls		
	Experiment (mm)	FEM (mm)	Relative error	Experiment (mm)	FEM (mm)	Relative error
1	30.2	29.08	0.037	32	31.81	0.006
2	30.5	29.14	0.044	32.55	32.16	0.012
3	30.2	29.04	0.038	32.7	32.2	0.015
4	30.05	29.12	0.031	32.5	31.44	0.033
5	25	23.41	0.064	26.1	25.63	0.018
6	25.1	23.24	0.074	26.8	25.63	0.044

Fig. 14 Relative error of walls distances between experiment and FEM

Relative error between experiment and FEM was defined in the form of Eq. (7):

$$Relative\ error = \frac{|D_{Exp} - D_{FEM}|}{D_{Exp}} \quad (7)$$

In Eq. (7), D_{Exp} and D_{FEM} refer to measured distance between walls in experiment and FEM, respectively. The plot of relative error according to positions is depicted in Fig. 14.

According to Fig. 14, relative error between experiment and FEM increases as position of measurement moves toward location between draw beads. Main reason for this increase is wear of draw beads. In order that, their height will become less than the size of model in FEM simulation. In this situation draw beads can't hold the blank and restraining force will decrease, so the thickness of elastic region in blank after drawing will increase which in turn will increase spring back. Comparing the relative error for top and bottom of the wall measurements shows that the bottom has higher relative error. Major reason is that part of the blank which forms top of the wall passes through the complex geometry and experiences more deformation and higher stress state so the effect of inadequate restraining force from draw beads

was compensated. The bottom of the wall has simple geometry and less deformation. Hence, wear of draw bead and insufficient restraining force affect this section more than top of the wall.

Next, the distances between the blank edges of the drawn part were measured at 5 points. The chosen edges were parallel to the part walls. Figure 15 shows the result of measurement. Corresponding data are shown in Table 6.

The relative error of measurements was defined in Eq. (8).

$$Relative\ error = \frac{|D_{Exp} - D_{FEM}|}{D_{exp}} \quad (8)$$

In Eq. (8), D_{Exp} and D_{FEM} are measured distance of edges in experiment and FEM, respectively. Figure 16 shows the diagram of relative error for measuring blank edges distances in FEM and experiment. The diagram reaches a peak at position 2 and 4. These positions are areas between draw beads. Wear of draw beads caused applied restraining force to reduce. Reduction in restraining force in these areas increases blank slippage and relative error between experiments with FEM.

In the last inspection for evaluating the model, the residual stress in the blank was measured by hole-drilling method

Fig. 15 Transverse distances between edges of drawn blank

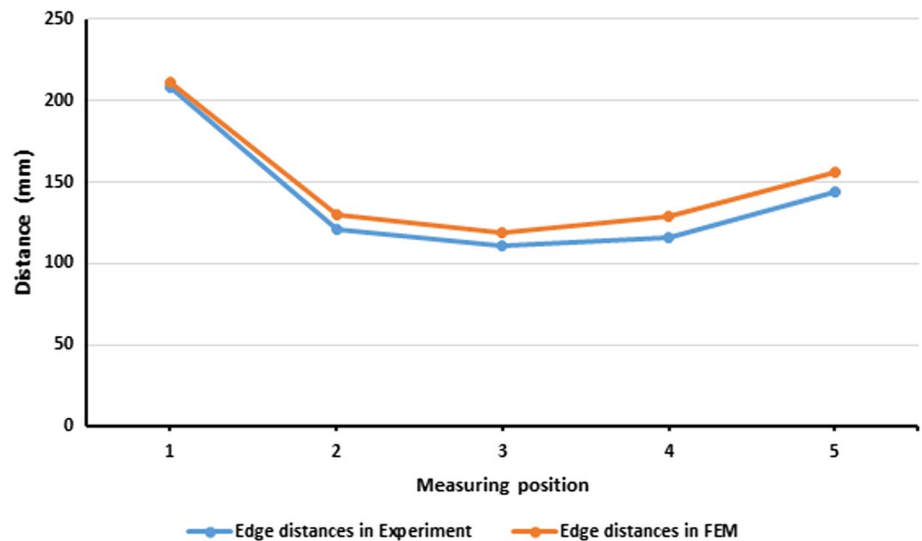


Table 6 Edges distances of drawn blank in experiment and FEM

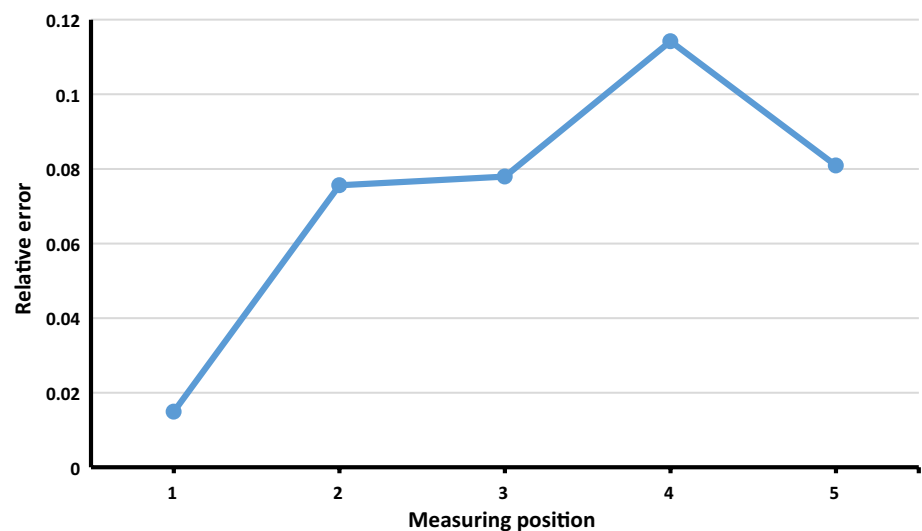
Point number	Edges distances in experiment (mm)	Edges distances in FEM (mm)	Relative error
1	208.45	211.56	0.015
2	121.3	130.47	0.076
3	110.5	119.11	0.078
4	116.2	129.47	0.114
5	144.5	156.19	0.081

and compared with model. The extent of residual stress in terms of normal and shear stress was measured in two positions as presented in Fig. 17a. Position 1 is on top of the drawn part; position 2 is past the bead cross section. Both positions are horizontal with Fig. 17b revealing position 2 on

the drawn part. Table 7 presents the results of experimental hole drilling test based on ASTM E837 standard along with FEM results.

According to Table 7, there is a considerable difference between experiment and FEM in residual stress component of σ_{zz} . The reason for this difference could be accumulation of residual stresses from previous process done on blank, like rolling and annealing. Raw material of deep drawing is cold-rolled steel. So the sheet which is used for deep drawing contains residual stress from previous processes. After deep drawing, the residual stress of this process accumulates on the residual stress of former processes with rule of superposition. In this situation measuring residual stress of drawn part reveals the residual stress of blank after rolling and drawing processes and this explains the difference between FEM and experiment.

Fig. 16 Relative error of edges distances in experiments and FEM



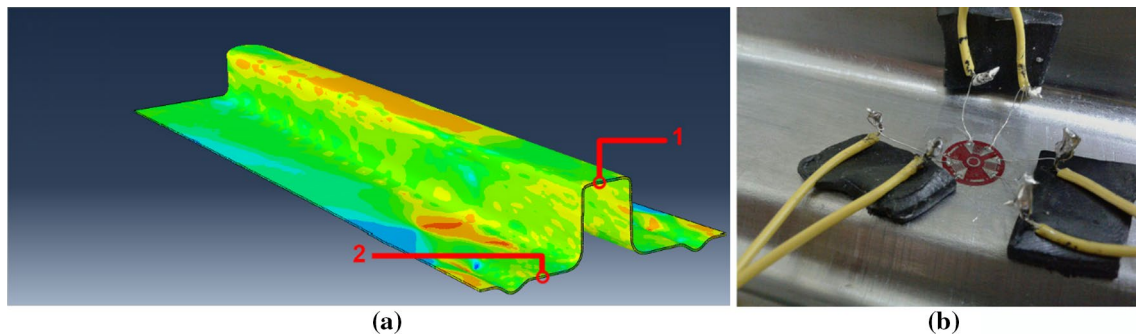


Fig. 17 Position of measured residual stress **a** finite element model **b** hole drilling of position 2

Table 7 Comparison of residual stresses for experiment and FEM

Position		σ_{xx} (MPa)	σ_{zz} (MPa)	σ_{xz} (MPa)
1	Experiment	61	15	4
	FEM	68.1	71.4	-1.1
2	Experiment	101	38	-2
	FEM	114.9	42.7	-1.2

Table 9 Acceptable ranges for dimensions of bead

Parameter	Symbol	Lower range	Upper range
Height	A	3	7
Width	B	7	13
Length	C	150	200

5 Optimization of deep drawing product

5.1 RSM method

After extracting the data of output parameters from 51 experiments suggested by Design-Expert, analysis of variance (ANOVA) was used to check whether each input parameter (or their combination) affected the output parameters. Thereafter, a set of input parameters which could produce a part with optimized output parameters was defined using RSM. For optimizing the deep drawing process, multi-objective optimizations for all parameters were carried out in the design expert software. In all situations of optimization, the criteria of optimization for the input parameters were set to lie within the ranges defined

in Table 1, and the importance of each output parameter was set equal to others. Then, for verification of RSM optimization results, the proposed bead was modeled and deep drawing process was simulated with the suggested coefficient of friction. For each coefficient of friction, the values of output parameters in multi-objective optimizations are provided in Table 8. The height, width, and length of the proposed bead are shown in the column of “proposed bead,” respectively.

5.2 RSM-GA method

Having applied RSM model, the obtained response surface for each output parameter was optimized using genetic algorithm (GA). After entering each response surface as a fitness

Table 8 Proposed points for outputs optimization in RSM

	Parameter	Proposed bead [height, width, length] (mm)	Maximum residual stress (MPa)		Maximum punch force (KN)		Maximum thinning (%)		Maximum wrinkling (mm)	
			RSM	FEM	RSM	FEM	RSM	FEM	RSM	FEM
$\mu=0.18$	Multi-O	[3.7, 13, 200]	284	315	125	160	0.12	0.13	2	2.19
	Current bead	[5, 5, 200]		325		376		0.20		1.85
$\mu=0.195$	Multi-O	[3.8, 13, 188]	298	309	168	589	0.14	0.14	1.95	1.68
	Current bead	[5, 5, 200]		339		843		0.18		1.07
$\mu=0.22$	Multi-O	[3.8, 7, 172]	292	299	176	181	0.22	0.27	1.8	1.24
	Current bead	[5, 5, 200]		323		811		0.20		1.62

Table 10 Proposed points for optimized outputs in RSM-GA and FEM

	Parameter	Proposed bead [height, width, length] (mm)	Maximum residual stress (MPa)		Maximum punch force (KN)		Maximum Thinning (%)		Maximum wrinkling (mm)	
			RSM-GA	FEM	RSM-GA	FEM	RSM-GA	FEM	RSM-GA	FEM
$\mu=0.18$	M-O	[3.7, 13, 200]	284	304	1.25	162	0.12	0.12	1.96	1.94
	Current bead	[5, 5, 200]		325		376		0.20		1.85
$\mu=0.195$	M-O	[4.1, 13, 192]	304	307	160	156	0.14	0.14	1.84	2.14
	Current bead	[5, 5, 200]		339		843		0.18		1.07
$\mu=0.22$	M-O	[4.1, 11.9, 195]	333	313	157	181	0.16	0.16	1.97	1.08
	Current bead	[5, 5, 200]		323		811		0.20		1.62

function for optimization in GA, the constraints required for optimization were defined. In this study, response surfaces had no equality or inequality constraints. There were only acceptable ranges for each input parameter which could be defined according to Table 9. Coefficient of friction (μ) was not included in this method as a variable in equations, since it was not a continuous variable and there was response surface for each μ . So, the equations of predicting output parameters were optimized for each level of friction separately.

To have multi-objective optimization at each level of μ , the summation of response surfaces was chosen as the function for optimization. For eliminating the dimension effect of each output parameter on its response surface, the response surfaces were nondimensionalized via dividing by maximum values observed in DOE chart. Accordingly, the multi-objective function for optimization was defined as follows (Eq. 9):

$$F_{MO} = \left(\frac{F_{RS}(x_1, x_2, x_3)}{MAX_{RS}} + \frac{F_{PF}(x_1, x_2, x_3)}{MAX_{PF}} + \frac{F_{Th}(x_1, x_2, x_3)}{MAX_{Th}} + \frac{F_{Wr}(x_1, x_2, x_3)}{MAX_{Wr}} \right). \quad (9)$$

After performing multi-objective optimization by genetic algorithm, the predicted values of optimization were compared with those from FEM, as observed in Table 10 (the optimized dimensions have been rounded up to one decimal place).

5.3 Comparison of results

After completion of optimizations by both methods, multi-objective results were selected for comparison. Since the optimization was defined separately on each level of μ , the values of output parameters of the current bead set up simulated with three quantities of μ were considered as criteria for comparison. The plots of relative values comparing the results of RSM and RSM-GA methods with those of the current experimental bead setup are illustrated in Fig. 18. Also, Table 11 shows the percentage of changes in output parameters via RSM and RSM-GA methods. According to this table, the dimensions suggested for the bead by means of

two methods were efficient in reducing the level of residual stress, punch force, and thinning, but led to higher extent of wrinkling. Note that the current dimensions of bead applied on the die were considered to minimize the wrinkling. Although in most of the suggested dimensions, increase in level of wrinkling was observed, for coefficient of friction of 0.22, the dimensions suggested by RSM-GA resulted in reductions in all four output parameters.

Comparison of results obtained from RSM and RSM-GA methods suggested that both methods could optimize the drawing quality, considering bead texture pattern alongside the geometry of bead as inputs of design. The capability of RSM-GA method for multi-objective optimization depends on the selected coefficients used for combination of response surfaces and creation of dimensionless function. The priority of optimization for different output parameters can be

adjusted by the value of coefficients considered for each case.

Based on Table 11, the values of punch force predicted by RSM and RSM-GA methods have had some differences from those measured by FE model. This can be attributed to ignoring the effect of other parameters such as forming speed or punch and die fillet radii. With regards to predicting and optimizing thinning, the proposed response surface could predict the maximum values of thinning. It can be concluded that essential parameters affecting the thinning were taken into account in the model. On the other hand, consideration of the other parameters such as punch and die fillet radii and drawing height on the model could enhance its accuracy. In case of elevation of the model accuracy for wrinkling, parameters such as punch speed, blank thickness, and blank holder force could also be considered in the model. Since the current setup of beads applied on the die was designed to minimize the wrinkling as a single-objective task, the other sets of design parameters mostly cause higher

Fig. 18 Plot of relative values that compare the results of both RSM and RSM-GA methods with current bead setup for **a** $\mu=0.18$ **b** $\mu=0.195$ **c** $\mu=0.22$

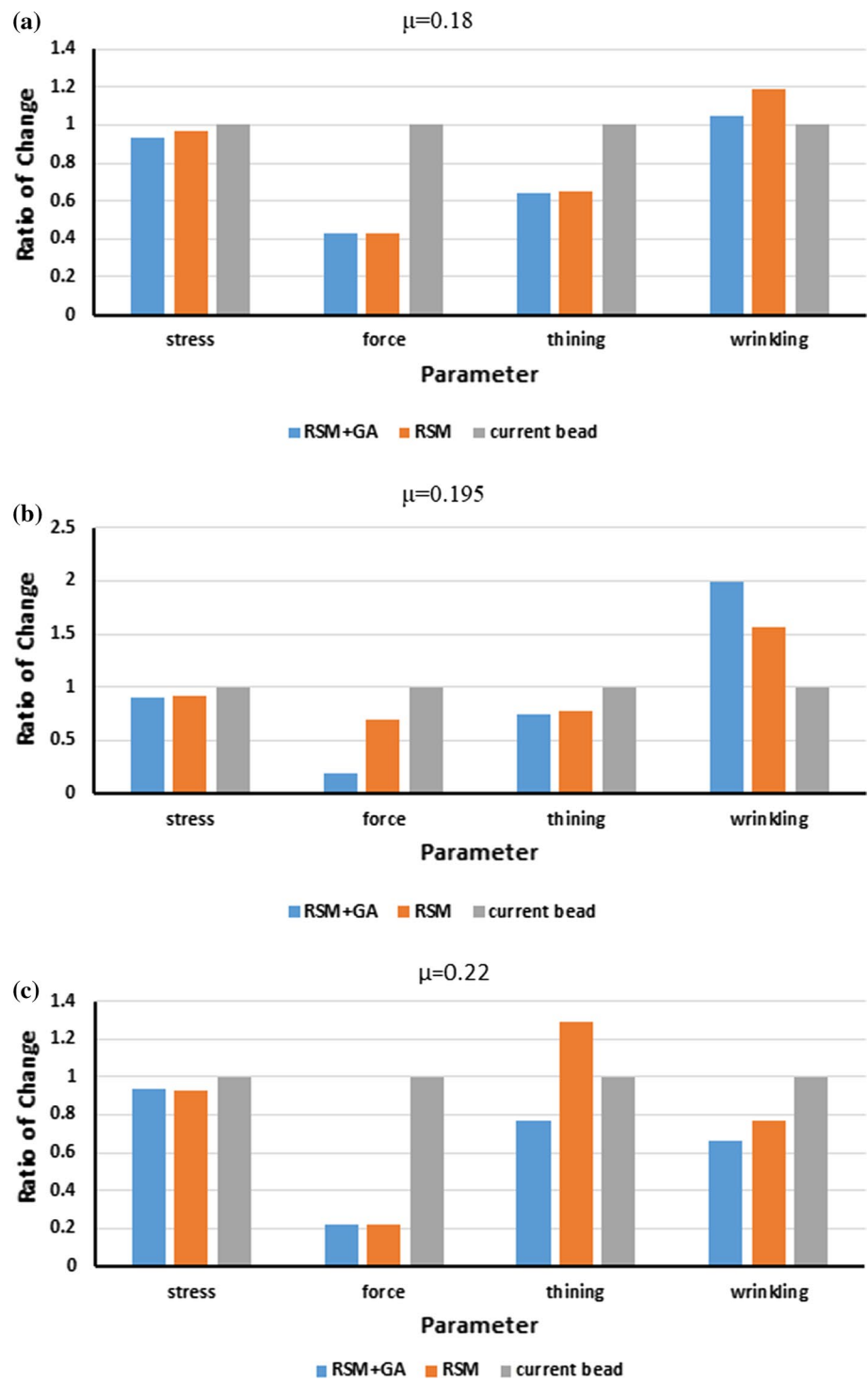


Table 11 Percentage of improvement in output parameters relative to current state of bead

Aim	$\mu=0.18$		$\mu=0.195$		$\mu=0.22$	
	RSM	RSM+GA	RSM	RSM+GA	RSM	RSM+GA
Residual Stress	2.9	6.3	9	9.4	7.3	6.2
Punch Force	57.5	56.9	30.1	81.4	77	77.6
Thinning	34.9	36.2	22.4	25.3	-29	23.5
Wrinkling	-18.6	-5	-56.3	-99	23.3	33.4

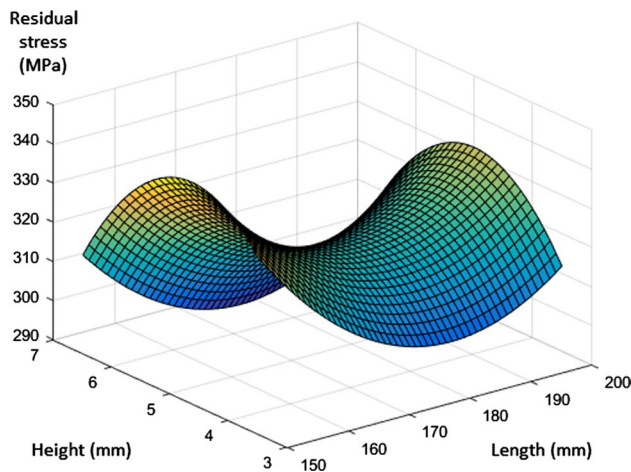


Fig. 19 Diagram of maximum residual stress vs. height and length for a draw bead in $\mu=0.18$

values for wrinkling. However, the optimization process for $\mu=0.22$ presented a point in the design space which reduced the wrinkling compared to the current bead setup. Finally, the proposed response surface could predict the extent of residual stress in the proposed points. Similarly, the punch speed, blank holder force, as well as punch and die fillet radii could be taken into account in the model to raise the accuracy.

5.4 Discussion on the relationship between inputs and outputs

A diagram was needed for each output to trace the change of each output parameter relative to the change in inputs. The 3-axis diagram was chosen for visualizing the change of residual stress in terms of input parameters, but in a certain amount of coefficient of friction, there were 3 input parameters, and only 2 of them could be used for diagram. So, the height and width of input were considered equal. Figure 19 shows the diagram of residual stress vs. height and length for a draw bead in $\mu=0.18$. Each point on the surface shows the residual stress of a draw bead with respect to the defined length and equal width and height size. According to Fig. 19, increasing the height and width of the draw bead increases the amount of residual stress. Increasing the length of the draw bead first decreases and then increases the amount of residual stress. Increasing the coefficient of friction just shifts the surface upward.

Figure 20 shows the diagram of thinning vs. height and length for a draw bead in $\mu=0.18$. According to Fig. 20, increasing the height and width of the draw bead first increases and then decreases the amount of thinning. Increasing the length of the draw bead decreases the amount of thinning. Similar to the residual stress diagram, increasing

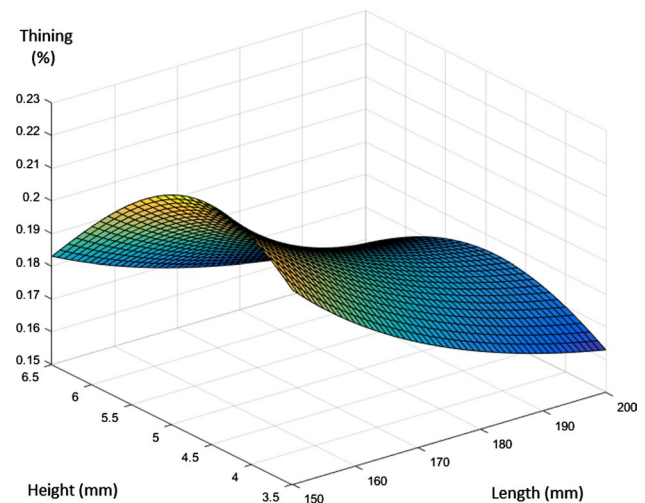


Fig. 20 Diagram of maximum thinning vs. height and length for a draw bead in $\mu=0.18$

the coefficient of friction shifts the thinning diagram upward. Figures 19 and 20 clearly show that residual stress and thinning have a saddle-type diagram, and using GA for optimizing these parameters was found to be more efficient than the classical optimization methods ($dy/dx=0$).

Figure 21 shows the diagram of wrinkling vs. height and length for a draw bead in $\mu=0.18$. According to Fig. 21, increasing the height and width of the draw bead first increases and then decreases the amount of wrinkling. It is the same regarding the increase in the length of the draw bead. Despite two former diagrams, although increasing the coefficient of friction increases the maximums of wrinkling, but in $\mu=0.195$ and $\mu=0.22$, the diagrams are mirrored horizontally relative to the $\mu=0.18$. This may be due to the change in material flow behavior.

When two surfaces contacting each other, two situations are probable. Situation 1: the interaction between plain areas of each surface leading to the adhesion of surfaces, and situation 2: the interaction between asperities of one surface with plain area or asperities of the other surface leading to the plowing. So, the friction force of two surfaces—during sliding—is the combination of shear force and plowing force between two surfaces. In this research, the results of measuring the coefficient of friction (Fig. 4) showed that, when machining tool path is parallel to the sliding direction of the sheet on the draw bead, the coefficient of friction is higher than the situation, in which the tool path is perpendicular to the sliding direction of the sheet on the draw bead, showing that in parallel machining, formed asperities are more inclined to plough the surface than the perpendicular machining. So, the plowing force and consequently friction force increased in the parallel situation. In case of combination of both machining strategies, the coefficient

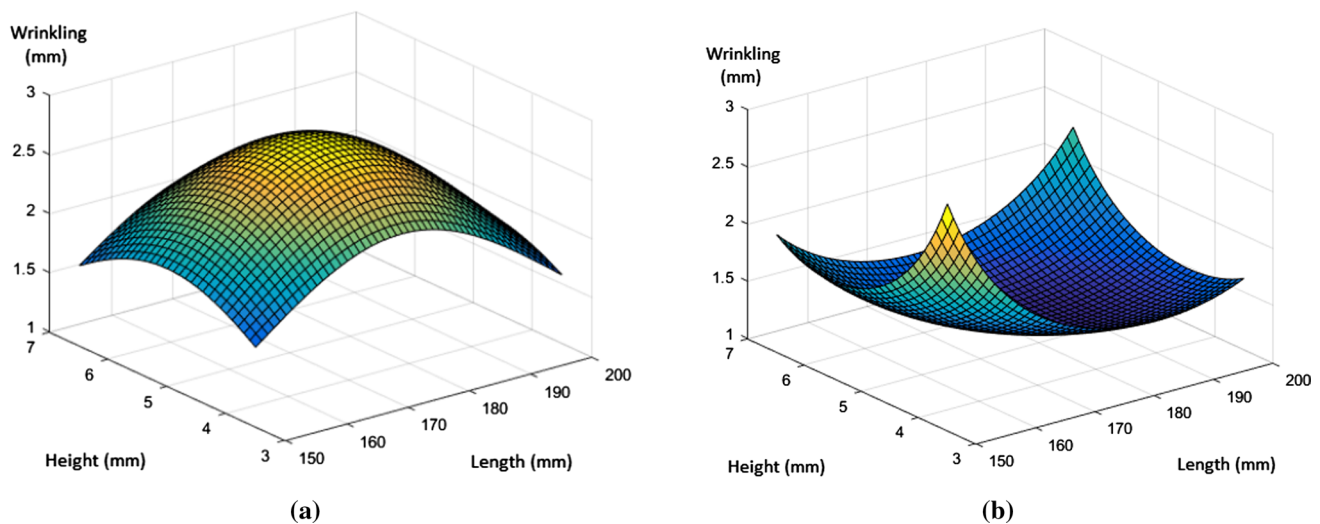


Fig. 21 Maximum wrinkling vs. height and length for a draw bead in **a** $\mu=0.18$ and **b** $\mu=0.195$

of friction was found to be the highest. Although the size and number of the asperities reduced in this situation, the size and number of the plain areas increased as well as the adhesion resulted between surfaces. Hence, it is concluded that this strategy causes an increase in the shear force and consequently the friction force. According to the explanations given about the surfaces contact, choosing the proper machining strategy and tool path overlap are considered as the major elements to create an appropriate surface texture, which in turn creates an appropriate combination of plain areas and asperities, making the desired level of coefficient of friction.

6 Conclusions

Texture pattern on surface of draw beads that is controlled by machining strategy is used along with the geometrical properties to design draw beads for an industrial drawing die. Analysis of optimization results, remarks that, inputting this parameter in design and applying RSM and GA methods to optimize the design was successful.

The process includes extracting material properties, FEM simulation, and comparison of one simulation with an experiment. The quality of drawn part was defined by 4 numerical parameters: maximum residual stress, maximum punch force, maximum thinning and maximum wrinkling, and the aim of design was set to achieving the optimum level of these parameters. Response surface method was used to design table of experiments. In addition, RSM and RSM-GA were used to find the optimum design. The results of optimization by RSM-GA showed that at one level of μ (certain machining strategy) and optimized bead dimension, the quality of drawn part was better than the current situation.

Although machining strategy is a good way to control the texture pattern on beads and the coefficient of friction, after hundreds or thousands of drawing, the pattern will disappear because of pressure and sliding of blank. Hence, the effect of this method is limited. Future studies should focus on coating the bead surface with chromium or PVD and CVD process and possible ways of texturing the coated surface to prolong the texture lifetime of draw beads.

Acknowledgements The authors highly appreciate the support of the Iran National Science Foundation (INSF). Further, the authors thank Mr. Shaghaghi and Mr. Moghadasi, chief and deputy of the press shop department of IranKhodro Diesel Industrial Group, who provided insight and expertise which greatly assisted us in the research.

Authors Contribution MM performed the measurements, CAD/CAE and optimization of results and wrote the manuscript. AP was the instructor and reviewer of the process and manuscript. All authors read and approved the final manuscript.

Funding The authors declare the support of the Iran National Science Foundation (INSF). The authors declare the Support of Iran Khodro Diesel Industrial Group for providing sheet samples, die and deep drawing products.

Availability of data and materials All deep drawing parts and sheet samples of this study are available from IranKhodro Diesel Industrial Group but restrictions apply to the availability of these objects, which were used under license for the current study, and so are not physically available. Data of stress–strain diagram of sheet samples and residual stress of deep drawing products are included in this published article. The datasets of RSM DOE, numerical results of DOE and optimizations, during the current study are not included in article due to not having any point and taking a lot of space in article, but are available from the corresponding author on request. All data generated on friction measurement and analyzed during comparison of results are included in this published article.

Code availability Optimization codes used in Matlab software are available if needed.

Declarations

Conflict of interest The authors of this article have registered the patent of measuring friction fixture introduced in this article. The authors of this article have not any financial and non-financial relation with Iran Khodro Diesel Industrial Group before, during and after the study. The authors of this article do not receive any financial and non-financial benefits from anyone or any group for study and publication of this study.

Ethics approval All research stages and data interpreted are carried out impartial. The foundation and cooperation of industry haven't had any effect on the results of investigation. All the previous information about the research and its sources is mentioned in the literature review and there is no use of data without mentioning the resource. Consent to participate All participants were involved in research of their own will and all are mentioned in authors section.

Consent of publish All the authors agreed to publish the results of research in the form of a paper.

References

- Li HX, Wen XZ, Nan Y (2011) Study on effect of draw bead on slip line of stamping part surface. *Mater Res Innov* 15:340–342
- Thipprakmas S (2011) Effect of draw bead height on wall features in rectangular deep-drawing process using finite element method. *Adv Mater Res* 264:1580–1585
- Phanitwong W, Thipprakmas S (2011) Analysis of draw bead geometry on wall thinning and concave/convex feature in rectangular deep drawn parts. *Adv Mater Res* 189:2704–2707
- Schey JA (1996) Friction and lubrication in drawing coated steel sheets on chromium-coated beads. *Lubr Eng* 52(9):677–681
- Raghavan KS, Narainen R, Smith LM (2013) Experimental and numerical study of restraining force development in inclined draw beads. *AIP Conf Proc* 1567(1):646–649
- Smith LM, Zhou YJ, Zhou DJ, Du C, Wanintrudal C (2009) A new experimental test apparatus for angle binder draw bead simulations. *J Mater Process Technol* 209(10):4942–4948
- Murali A, Gopal M, Rajadurai A (2010) Analysis of Influence of draw bead location and profile in hemispherical cup forming. *IACSIT Int J Eng Technol* 2(4):356–360
- Sheriff N, Ismail M (2008) Numerical design optimisation of drawbead position and experimental validation of cup drawing process. *J Mater Process Technol* 206(1):83–91
- Chen FK, Liu JH (1997) Analysis of an equivalent draw bead model for the finite element simulation of a stamping process. *Int J Mach Tools Manuf* 37(4):409–423
- Naceur HY, Guo Q, Batoz JL, Knopf-Lenoir C (2001) Optimization of drawbead restraining forces and drawbead design in sheet metal forming process. *Int J Mech Sci* 43(10):2407–2434
- Wei L, Yang Y (2008) Multi-objective optimization of sheet metal forming process using Pareto-based genetic algorithm. *J Mater Process Technol* 208(1):499–506
- Sun G, Li G, Gong Z, Cui X, Yang X, Li Q (2010) Multi-objective robust optimization method for drawbead design in sheet metal forming. *Mater Des* 31(4):1917–1929
- Han LF, Li GY, Han X, Zhong ZH (2006) Identification of geometric parameters of drawbead in metal forming processes. *Inverse Probl Sci Eng* 14(3):233–244
- Han X, Wang G, Liu GP (2009) A modified Tikhonov regularization method for parameter estimations of a drawbead model. *Inverse Probl Sci Eng* 17(4):437–449
- Hu W, Li E, Yao LG (2010) Parallel boundary and best neighbor searching sampling algorithm for drawbead design optimization in sheet metal forming. *Struct Multidiscip Optim* 41(2):309–324
- Kardan M, Parvizi A, Askari A (2018) Experimental and finite element results for optimization of punch force and thickness distribution in deep drawing process. *Arab J Sci Eng* 43:1165–1175
- Kardan M, Parvizi A, Askari A (2018) Influence of process parameters on residual stresses in deep-drawing process with FEM and experimental evaluations. *J Braz Soc Mech Sci Eng*. <https://doi.org/10.1007/s40430-018-1085-9>
- Lee BH, Keum YT, Wagoner RH (2002) Modeling of the friction caused by lubrication and surface roughness in sheet metal forming. *J Mater Process Technol* 130:60–63
- ASTM G115–10 (2013) Standard guide for measuring and reporting friction coefficients. ASTM International, West Conshohocken. www.astm.org. Accessed 1 Aug 2017

Publisher's Note Springer Nature remains neutral with regard to jurisdictional claims in published maps and institutional affiliations.